Experimental Evaluation of Adaptive Doppler Estimation for PRI-Staggered Radar

Lumumba A. Harnett, Brandon Ravenscroft, Shannon D. Blunt, Christopher T. Allen
Radar Systems Lab (RSL), University of Kansas (KU), Lawrence, KS

***Abstract*—Doppler processing enables pulse-Doppler radar to cancel clutter and discriminate movers based on their relative radial motion by exploiting slow-time signal coherence across the pulses of a radar dwell. Where the unambiguous Doppler interval is bounded by half the pulse repetition frequency (PRF) when the set of pulse repetition intervals (PRIs) are uniform, the use of staggered PRIs is known to expand this interval according to the least common multiple of the various PRFs involved. Of course, doing so also alters the periodic-sinc Doppler response into structures that may possess disadvantageously high sidelobes, particularly when the PRIs are randomized, and this condition cannot be readily addressed through tapering like in the uniform case. Consequently, we examine application of the reiterative super-resolution (RISR) robust beamforming approach to this spectral estimation problem, demonstrating its utility using open-air measurements in conjunction with clutter cancellation.**

Keywords—Doppler processing, adaptive estimation, PRI staggering

I. Introduction

Doppler processing is instrumental to the discrimination between movers and clutter for moving target indication (MTI) radar based on radial motion relative to the platform. For the standard coherent processing interval (CPI) of uniform PRIs, the result is superposition of periodic-sinc responses corresponding to the illuminated scattering velocities. Uniformity in the CPI is convenient from a receive processing computational standpoint, but doing so also introduces the well-known trade-space between unambiguous range and Doppler (velocity) that is dictated by the PRI and its inverse counterpart the PRF, respectively [1]. The ambiguity in velocity is a result of PRI periodicity, such that Doppler frequencies outside the unambiguous interval of [–PRF/2, +PRF/2] are aliased back into this interval. That said, it is this periodicity that permits application of the efficient fast Fourier transform (FFT).

In contrast, random PRI staggering varies the PRI extent on a pulse-to-pulse basis over the CPI, thereby yielding an unambiguous Doppler spectrum [1]. The effects of non-uniform slow-time sampling for PRI-staggered radar were first examined for Doppler processing as early as the 1970s (e.g. [2-4]). In general, PRI staggering can unmask Doppler-aliased movers, albeit with the tendency for a higher and flatter Doppler response than periodic-sinc. Staggering also imposes a non-uniform slow-time sampling that necessitates modification to the uniformly sampled discrete Fourier transform (DFT), though efficient forms do exist [5]. Of course, this modification also precludes the use of simple tapering to mitigate Doppler sidelobes.

Because the staggering sequence is known precisely by the radar, and corresponding Doppler steering vectors can thus be readily constructed, this problem lends itself to adaptive receive processing methods that perform recursive sidelobe suppression using a structured model. In recent years, various methods have been developed and examined in simulation (e.g. [6-8]), and it is only quite recently that experimental results have begun to emerge [9], with the latter applying compressive sensing techniques. Here we consider a variant of reiterative minimum mean-square error (RMMSE) estimation first developed for pulse compression [10], which has evolved to become quite robust to physical phenomenology and has been demonstrated experimentally for multiple sensing applications (e.g. [11-14]).

The particular version of RMMSE employed here relies on a beamforming approach previously denoted as reiterative superresolution (RISR) [15], which was subsequently generalized to incorporate a "partial" gain constraint [16] to improve practical performance. Here RISR is instead used to perform adaptive spectral estimation on each individual range snapshot composed of slow-time samples, with the adaptive response yielding enhanced Doppler separability of clutter/movers and sidelobe suppression to improve subsequent detection sensitivity. Different forms of this same approach have recently been developed and experimentally demonstrated for stretch processing [12] and joint clutter cancellation and signal estimation [14], with concurrent papers [17, 18] demonstrating open-air adaptive direction finding (along with array self-calibration) and subsequent signal characterization via an adaptive spectrogram formulation. Here we show how this robust processing approach can expand the utility of PRI staggering, particularly in combination with clutter cancellation.

II. PRI-Staggered Radar Signal Model

Consider a pulse-Doppler radar transmitting M pulses in a CPI, where the mth PRI, denoted as $T_{m,}$ varies (or "staggers") on a pulse-to-pulse basis. Each pulse is modulated by waveform $s(t)$ having pulse width τ and 3-dB bandwidth B. The resulting scattering captured at the radar receiver (subsuming beamforming) for the mth pulse is therefore

$$y(m,t) = \sum_{f_\mathrm{D}} \left[s(t) * x(t;\, f_\mathrm{D}) \right] e^{j2\pi f_\mathrm{D} T_\mathrm{acc}(m)} + n(m,t) \qquad (1)$$

for fast-time PRI interval $t \in [0, T_m]$, where $x(t; f_\mathrm{D})$ is the scattering response according to Doppler frequency f_D (ignoring fast-time Doppler effects), $*$ denotes convolution, and $n(m,t)$ is thermal noise assumed to be white Gaussian with zero-mean and variance (noise power) σ_n^2. The term

$$T_\mathrm{acc}(m) = \sum_{q=0}^{m-1} T_q \qquad (2)$$

This work was supported by the Office of Naval Research under Contract #N00014-20-C-1006. DISTRIBUTION STATEMENT A. Approved for Public Release.

is the accumulated time prior to the mth PRI, where $T_0 = 0$ and $T_{acc}(1) = 0$ for the first pulse. The mth PRI can be expressed as

$$T_m = T_{avg} + \Delta T_m \tag{3}$$

where deviation ΔT_m is independently drawn from the fixed interval $[-\delta, +\delta]$ and the average PRI is simply

$$T_{avg} = \frac{1}{M} \sum_{m=1}^{M} T_m \,. \tag{4}$$

Pulse compression is applied to (1) via

$$z(m,t) = h(t) * y(m,t) \tag{5}$$

for $h(t)$ the matched (or mismatched [11]) filter yielding a signal-to-noise ratio (SNR) gain commensurate with the waveform time-bandwidth product (τB). After discretization, the collection of M slow-time samples at the ℓth range bin is

$$\begin{aligned} \mathbf{z}(\ell) &= \sum_{f_D} \tilde{x}(\ell;\, f_D)\mathbf{v}(f_D) + \tilde{\mathbf{n}}(\ell) \\ &\cong \mathbf{V}\tilde{\mathbf{x}}(\ell) + \tilde{\mathbf{n}}(\ell) \end{aligned} \tag{6}$$

in which $\tilde{x}(\ell;\, f_D)$ subsumes the effects of pulse compression and discretization in Doppler as indicated by $\cong$ due to ensuing approximation error. The discretized signal model in (6) contains the $M \times 1$ Doppler steering vector

$$\mathbf{v}(f_D) = \begin{bmatrix} 1 & e^{j2\pi f_D T_{acc}(2)} & \cdots & e^{j2\pi f_D T_{acc}(M)} \end{bmatrix}^T , \tag{7}$$

where $(\cdot)^T$ is the transpose operation and the $M \times N$ matrix $\mathbf{V}$ collects these steering vectors into the columns according to some specified granularity over a physically meaningful Doppler interval. The associated $N \times 1$ vector $\tilde{\mathbf{x}}(\ell)$ is therefore comprised of scattering values at the ℓth range cell discretized in Doppler in the same manner as $\mathbf{V}$, and with $M \times 1$ vector $\tilde{\mathbf{n}}(\ell)$ containing samples of noise.

For M pulses in the CPI, $N = M$ is the nominal level of Doppler discretization, and thus $N = KM$ for oversampling factor $K \geq 1$ provides better visibility and reduced Doppler straddling. The fidelity benefit of the latter is particularly important for enhancement via adaptive estimation. Setting $\mathbf{W}_{DP} = (1/M)\,\mathbf{V}$ thus permits standard Doppler processing as

$$\hat{\mathbf{x}}_{DP}(\ell) = \mathbf{W}_{DP}^H \mathbf{z}(\ell)\,, \tag{8}$$

where $(\cdot)^H$ is the complex-conjugate transpose (Hermitian) operation and scattering responses within $N \times 1$ vector $\hat{\mathbf{x}}_{DP}(\ell)$ have experienced an SNR gain of M via coherent matching.

For uniform PRIs this Doppler processing response takes the form of a periodic-sinc function, the high sidelobes of which (the largest around −13 dB) are generally addressed by incorporating a taper via $\mathbf{w}_{DP}(f_D) \odot \mathbf{b}$, where $\mathbf{b}$ is some window function (e.g. Taylor, Hamming, etc) and $\odot$ denotes the Hadamard product [1]. Tapering does introduce some mainlobe broadening and SNR loss according to the particular taper, though these effects are generally acceptable given the significant sidelobe reduction obtained in the trade. However, tapering is not applicable to arbitrary PRI staggering.

In the uniform PRI case there is a single PRF that equates to $1/T_{avg}$, with unambiguous Doppler interval [–PRF/2, +PRF/2], meaning that mover responses outside this interval get aliased. It is well known [1] that PRI staggering extends the interval of unambiguous Doppler by the factor

$$\beta = T_{avg}\, \mathrm{LCM}\{\, f_1,\, f_2, \cdots,\, f_M \,\}\,, \tag{9}$$

in which LCM{·} denotes the least common multiple of the arguments and $f_m = 1/T_m$. In the uniform case (9) simplifies to $\beta = T_{avg}(1/T_{avg}) = 1$, while staggering yields $\beta > 1$. Since β could be quite large for some staggering sequences, let β_{mov} denote the factor that includes all expected mover velocities. Thus, the overall number of columns in the filter bank is $N = \beta_{mov} KM$.

Given that the $\beta = 1$ (uniform) case involves a repetition of the Doppler mainlobe (i.e. perfectly coherent) at every multiple of the PRF, this extension of unambiguous Doppler amounts to a form of "conservation of ambiguity" in which the randomized Doppler sidelobes flatten to a level that (in the expectation) is $1/M$ below the mainlobe peak. An example of this trade-off is illustrated in Fig. 1 for $M = 30$, where the mainlobe at zero Doppler (e.g. for clutter) is repeated every multiple of the PRF for the uniform PRI case (blue trace). We see that tapering by a −40 dB Taylor window (green trace) provides significant sidelobe reduction, though the ambiguity remains. In contrast, the response for a random instantiation of staggered PRI (red trace) does not recohere into repeated peaks, though the sidelobes are generally higher as a trade-off, and application of the taper (black trace) yields no benefit.

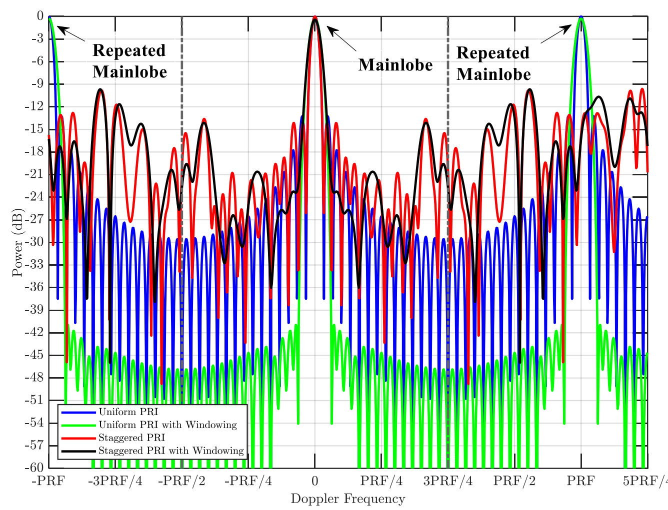

Fig. 1: Normalized Doppler response for a point scatterer at zero-Doppler for uniform PRI (with and without tapering) and randomly staggered PRI (with and without tapering)

III. RMMSE Adaptive Doppler Estimation

Using the Doppler signal structure from (6), which is mathematically identical to the beamforming problem, the corresponding RISR form of RMMSE [15] is realized via the mean-square error (MSE) cost function

$$J_{MSE}(\ell, f_D) = E\left[\, \left| \,\tilde{x}(\ell;\, f_D) - \mathbf{w}^H(\ell, f_D)\, \mathbf{z}(\ell) \right|^2 \right], \tag{10}$$

where $E[\cdot]$ denotes expectation. The solution is readily obtained by determining the gradient of (10) with respect to $\mathbf{w}(\ell, f_D)$, equating to zero, and then solving for the filter, which yields

$$\mathbf{w}_{\mathrm{U}}(\ell, f_{\mathrm{D}}) = \left(E\left[\mathbf{z}(\ell)\mathbf{z}^{H}(\ell)\right]\right)^{-1} E\left[\tilde{x}^{*}(\ell; f_{\mathrm{D}})\,\mathbf{z}(\ell)\right]$$
$$= \left(\mathbf{V}\mathbf{P}(\ell)\mathbf{V}^{H} + \mathbf{R}_{\mathrm{n}}\right)^{-1} \mathbf{v}(f_{\mathrm{D}})\,\rho(\ell, f_{\mathrm{D}}) \tag{11}$$
$$= \mathbf{D}^{-1}(\ell)\,\mathbf{v}(f_{\mathrm{D}})\,\rho(\ell, f_{\mathrm{D}}),$$

with the subscript U denoting "unconstrained". Here $\rho(\ell, f_{\mathrm{D}}) = E[|\,\tilde{x}(\ell, f_{\mathrm{D}})\,|^{2}]$ is the expected power in the given range/Doppler cell, which is collected into the $N \times N$ diagonal matrix $\mathbf{P}(\ell) = [\tilde{\mathbf{x}}(\ell)\tilde{\mathbf{x}}^{H}(\ell)]$ comprising the power spectrum, based on the assumption that components of $\tilde{\mathbf{x}}(\ell)$ are independent and zero-mean random processes. Likewise, $\mathbf{R}_{\mathrm{n}} = E[\tilde{\mathbf{n}}(\ell)\tilde{\mathbf{n}}^{H}(\ell)] = \sigma_{\mathrm{n}}^{2}\mathbf{I}$ is the $M \times M$ noise covariance matrix under the white noise assumption. Note that the $M \times M$ matrix $\mathbf{D}(\ell)$ collects the terms within the inverse for compact representation and the complete $M \times N$ filter bank $\mathbf{W}(\ell)$ is formed by collecting the N filters $\mathbf{w}_{\mathrm{U}}(\ell, f_{\mathrm{D}})$ across discretized Doppler. Further, the values $\rho(\ell, f_{\mathrm{D}})$ are not known *a priori* and are instead estimated in a recursive manner.

In [16], the RISR formulation was modified to incorporate a unity gain constraint (GC), yielding the form

$$\mathbf{w}_{\mathrm{GC}}(\ell, f_{\mathrm{D}}) = \frac{1}{\mathbf{v}^{H}(f_{\mathrm{D}})\,\mathbf{D}^{-1}(\ell)\,\mathbf{v}(f_{\mathrm{D}})}\,\mathbf{D}^{-1}(\ell)\,\mathbf{v}(f_{\mathrm{D}}) \tag{12}$$

for this spectrum estimation context, which appears similar to the minimum variance distortionless response (MVDR), though the implementation is different. The unconstrained and gain-constrained RISR filters from (11) and (12) were then combined in [16] to realize the "partially constrained" (PC) form

$$\mathbf{w}_{\mathrm{PC}}(\ell, f_{\mathrm{D}}) = \frac{\left(\rho(\ell, f_{\mathrm{D}})\right)^{1-\alpha}}{\left(\mathbf{v}^{H}(f_{\mathrm{D}})\,\mathbf{D}^{-1}(\ell)\,\mathbf{v}(f_{\mathrm{D}})\right)^{\alpha}}\,\mathbf{D}^{-1}(\ell)\,\mathbf{v}(f_{\mathrm{D}}) \tag{13}$$

for $0 \le \alpha \le 1$ an exponential weighting factor permitting a trade-off between unconstrained and fully constrained operation. The utility of this trade-off arises from the behavior of the two forms. The unconstrained version in (11) provides significant super-resolution enhancement, but has the tendency to suppress signals with lower SNR and does not provide a meaningful noise floor for subsequent detection processing. In contrast, the fully constrained version in (12) preserves low SNR signals and does provide a noise floor, though the degree of super-resolution is more modest. Thus, the geometric ratio combination in (13) establishes a simple way to determine a useful middle ground. As before, the $M \times N$ filter bank $\mathbf{W}(\ell)$ is formed by collecting the N filters from (12) or (13) across discretized Doppler.

The filters in (11)-(13) are all implemented in a recursive fashion by first applying standard Doppler processing via (8) and denoting $\hat{\mathbf{x}}_{i=0}(\ell) = \hat{\mathbf{x}}_{\mathrm{DP}}(\ell)$ as the initialization. For $i = 1, \ldots, I_{\mathrm{iter}}$ iterations, the RISR Doppler estimation process then involves the sequence of steps consisting of estimating the revised power spectrum matrix

$$\hat{\mathbf{P}}_{i}(\ell) = [\hat{\mathbf{x}}_{i-1}(\ell)\hat{\mathbf{x}}_{i-1}^{H}(\ell)] \odot \mathbf{I}_{N\times N}, \tag{14}$$

updating the $M \times N$ filter bank $\mathbf{W}_{i}(\ell)$ via (11), (12), or (13), and then applying the filter bank as

$$\hat{\mathbf{x}}_{i}(\ell) = \mathbf{W}_{i}^{H}(\ell)\,\mathbf{z}(\ell) \tag{15}$$

to update the Doppler estimate. Note that this process is performed independently for each range index ℓ, meaning that unlike traditional spectral estimation methods involving determination of a sample covariance matrix – e.g. standard MVDR, MUSIC, etc. – RISR is applied on a per-snapshot basis.

As suggested in [14], it is also possible to replace $\mathbf{z}(\ell)$ in (8) and (15) with the interference-cancelled form

$$\mathbf{a}(\ell) = \mathbf{R}_{\mathrm{canc}}^{-1}(\ell)\,\mathbf{z}(\ell), \tag{16}$$

where

$$\mathbf{R}_{\mathrm{canc}}(\ell) = \mathbf{R}_{\mathrm{clut}}(\ell) + \mathbf{R}_{\mathrm{int}}(\ell) + \mathbf{R}_{\mathrm{nse}}(\ell) \tag{17}$$

is a cancellation matrix comprised of clutter, interference, and noise covariance matrices. In other words, adaptive estimation using RISR can be performed either before or after cancellation to enhance Doppler processing. The following examines the efficacy of this approach on measured data.

IV. Experimental Validation

Open-air experimental measurements were collected at the University of Kansas using both uniform and staggered PRI arrangements. An LFM waveform with time-bandwidth product $\tau B = 150$ was used in both cases, with each containing 1200 pulses organized into 30 sub-CPIs of 40 pulses having the same PRI. For the uniform case the 30 sub-CPIs are identical, while for the staggering case each group of 40 pulses possess the same staggering, which is otherwise random across the CPI. The full sets of 1200 pulses were range/Doppler processed to establish a high-gain ground truth for the movers present. The two sets of pulses were transmitted sequentially at a center frequency of 3.55 GHz so that the illuminated scene is nearly identical.

To illustrate the effect of extending unambiguous velocity, only the first 4 pulses out of each sub-CPI were pre-summed after pulse compression (for 6 dB SNR gain) so that the result serves as an effective CPI of $M = 30$ pulses for each arrangement (uniform and staggered) with an effective average PRF of 80 Hz. Consequently, unambiguous velocity for the uniform PRI case amounts to ±1.7 m/s. Aside from determining ground truth, the remaining 36 pulses in each sub-CPI were not used.

The radar mainbeam was pointed toward the intersection of 23rd and Iowa Streets in Lawrence, KS that is about 1.1 km in range. Fig. 2 shows the hardware set-up and illuminated field of view. The rather low unambiguous velocity was purposely selected to show how movers in this scene get aliased, where the speed limit is 40 mph = 17.9 m/s. After I/Q sampling and pulse compression the movers within the beam extend over an interval of roughly 300 m. Using the full 1200-pulse uniform CPI, which has an actual PRF = 3.2 kHz, the fastest mover during the illumination time (soon after a stoplight change) was observed to be ~14 m/s.

In the following results, Doppler is over-sampled by $K = 5$, yielding 5×30 = 150 discretized Doppler frequency bins for each unambiguous Doppler interval, which is further extended by $\beta_{\mathrm{mov}} = 16$ to $N = 150\times16 = 2400$. The estimated noise power of −75 dBm was obtained from the pulse compressed data prior to Doppler processing. Here the PC-RISR version from (13) was employed, with the exponential weighting factor α set to 0.8 and $I_{\mathrm{iter}} = 10$ iterations performed.

Fig. 2: Hardware setup (top) and annotated field of view (bottom, courtesy of Google Earth) for open-air measurements. The yellow circles denote the location of the traffic intersection.

Effective ground truth was obtained by processing the entire 1200-pulse CPI of uniform PRIs without pre-summing, with the actual PRF = 3.2 kHz easily sufficient to observe all movers without aliasing. Further, because 10× more pulses are being coherently processed compared to the results that follow, the scattering responses are also 10 dB higher in this case. Figs. 3 and 4 illustrate this ground truth case without and with clutter cancellation, respectively, where the latter uses a simple projection at/around zero Doppler (due to the stationary platform). Figs. 5 and 6 likewise show ground truth for the entire 1200-pulse CPI of staggered PRIs without pre-summing, with the uniform and staggered cases collected back-to-back to enable comparison. We observe what appears to be 5 or 6 larger movers from roughly 1130m to 1185m that are traveling between 5 and 11 m/s, and perhaps 5 others movers having more modest SNR.

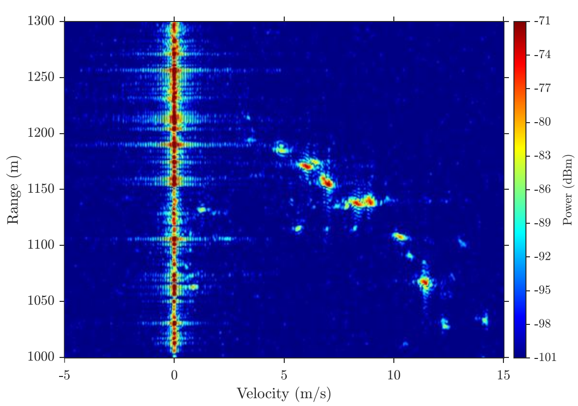

Fig. 3: Open-air MTI response after standard Doppler processing for uniform PRI of 3.2 kHz PRF

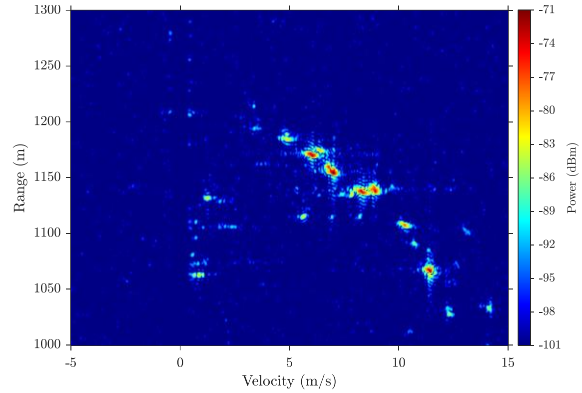

Fig. 4: Open-air MTI response after standard Doppler processing and clutter cancellation for uniform PRI of 3.2 kHz PRF

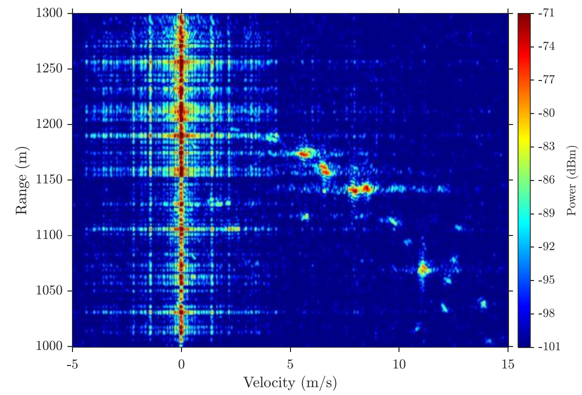

Fig. 5: Open-air MTI response after standard Doppler processing for staggered PRI of 3.2 kHz PRF

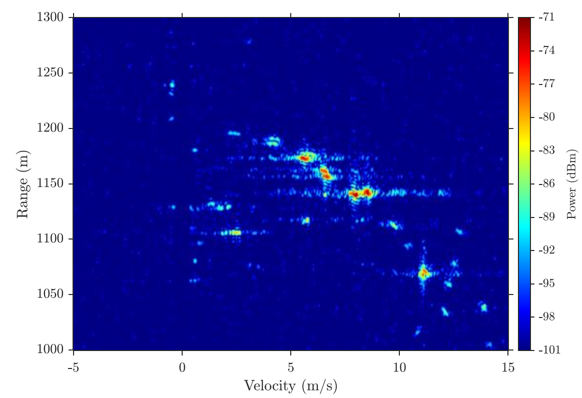

Fig. 6: Open-air MTI response after standard Doppler processing and clutter cancellation for staggered PRI of 3.2 kHz PRF

Now consider pre-summing of the uniform PRIs (only first 4 pulses of each sub-CPI) to obtain 30 effective pulses at an effective PRF of 80 Hz. Figs. 7 and 8 show the outcome of standard Doppler processing and adaptive Doppler processing using RISR, respectively. In both we see the repeated structure and clear foldover in Doppler due to aliasing (compared to Figs. 3 and 4), with the aliased portions outlined in pink dashed boxes. Aliasing notwithstanding, the RISR response in Fig. 8 does show the practical realization of Doppler super-resolution and sidelobe suppression that can benefit subsequent detection processing. Also note the expected 10 dB lower SNR since only 1/10$^{\text{th}}$ of the 1200 pulses are now being used.

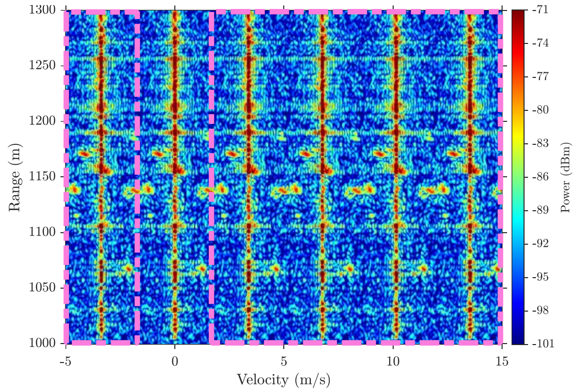

Fig. 7: Open-air MTI response after standard Doppler processing for uniform PRI, aliased due to low effective PRF of 80 Hz (aliased portions in pink)

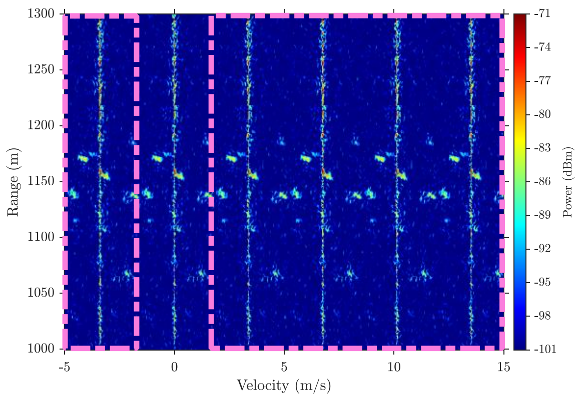

Fig. 8: Open-air MTI response after adaptive Doppler processing via RISR for uniform PRI, aliased due to low effective PRF of 80 Hz (aliased portions in pink)

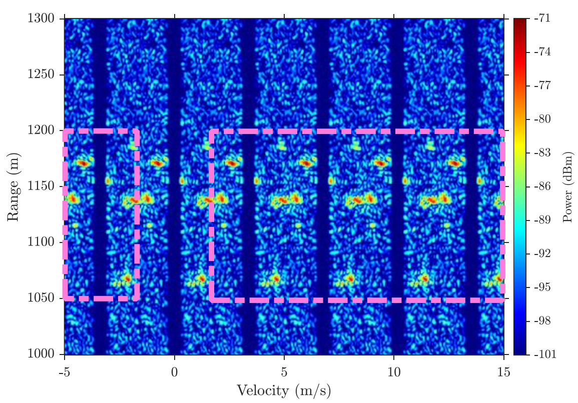

Fig. 9: Open-air MTI response after standard Doppler processing and clutter cancellation for uniform PRI, aliased due to low effective PRF of 80 Hz (aliased portions circled in pink)

Figs. 9 and 10 likewise illustrate standard and adaptive processing for the uniform PRI case after clutter cancellation via (16). Comparing Figs. 7 and 9 we see that suppressing clutter combined with standard processing improves visibility of movers as expected, though the adaptive processing results via RISR in Figs. 8 and 10 reveal significant visibility enhancement by concentrating response energy and suppressing the sidelobe background, which again translates into better subsequent detection capability. Indeed, for the movers that have been identified, a few dB improvement is obtained in terms of mover SNR relative to the surrounding noise floor when adaptive Doppler processing is used.

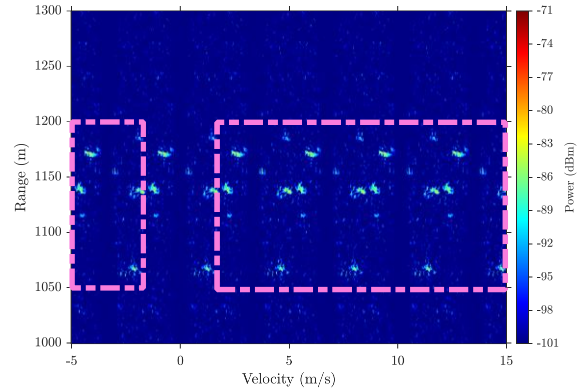

Fig. 10: Open-air MTI response after adaptive Doppler processing via RISR and clutter cancellation for uniform PRI, aliased due to low effective PRF of 80 Hz (aliased portions circled in pink)

Figs. 11 and 12 then depict standard and adaptive Doppler processing for the staggered PRI arrangement, which also has an average effective PRF = 80 Hz. Fig. 11 is clearly far less discernible for movers (due to high Doppler sidelobes) relative to the corresponding uniform PRI case in Fig. 7. However, the RISR adaptive response to staggered PRI in Fig. 12 shows significant sidelobe suppression and Doppler super-resolution, thereby revealing all the movers at their correct velocities.

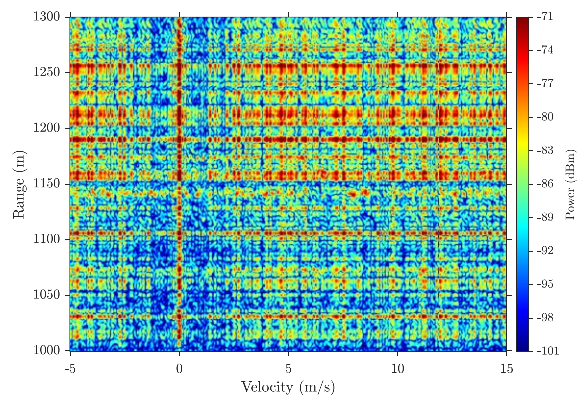

Fig. 11: Open-air MTI response after standard Doppler processing for staggered PRI with average effective PRF of 80 Hz

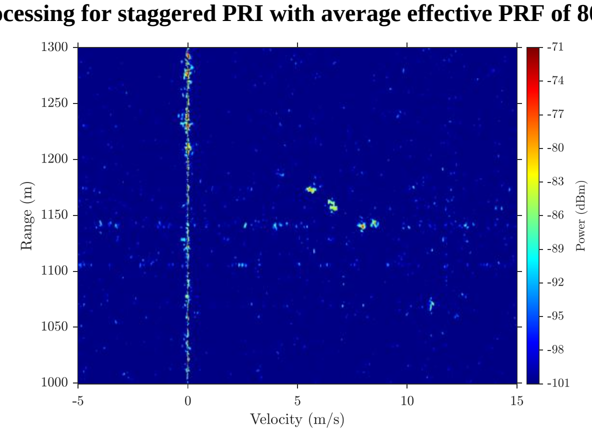

Fig. 12: Open-air MTI response after adaptive Doppler processing via RISR for staggered PRI with average effective PRF of 80 Hz

Similar behavior is observed in Figs. 13 and 14 when clutter cancellation is performed, though the former has noticeably better mover visibility than Fig. 11 due to clutter suppression. As a result, the adaptive Doppler response in Fig. 14 is almost negligibly different to that in Fig. 12, suggesting clutter cancellation may have limited efficacy in this context. That said, these results do not represent clutter scenarios with high dynamic range, meaning there is reason to expect the combination of clutter cancellation and adaptive Doppler processing to remain useful in such cases.

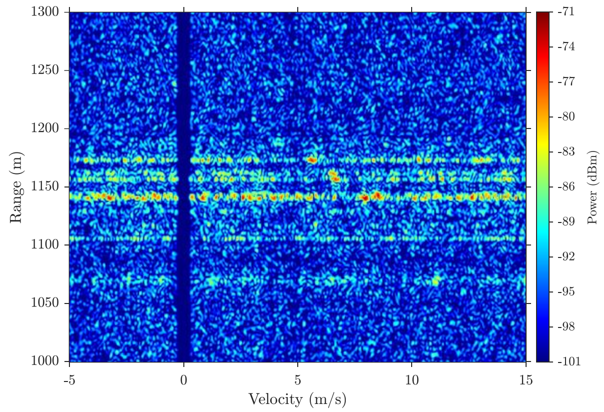

Fig. 13: Open-air MTI response after standard Doppler processing and clutter cancellation for staggered PRI with average effective PRF of 80 Hz

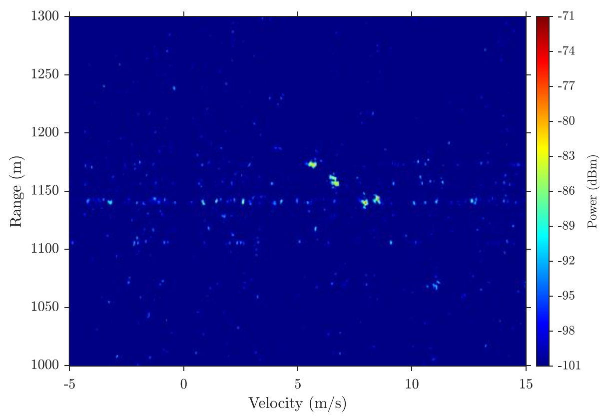

Fig. 14: Open-air MTI response after adaptive Doppler processing via RISR and clutter cancellation for staggered PRI with average effective PRF of 80 Hz

Comparing the results in Figs. 7-14 with the ground truth results in Figs. 3-6 we of course note that the uniform case (Figs. 7-10) experiences significant Doppler aliasing as expected. Standard processing for PRI staggering (Fig. 11 and 13) alleviates this aliasing, but at the price of high Doppler sidelobes that cannot be addressed through tapering. However, adaptive Doppler processing via RISR (Fig. 12 and 14) is found to provide an effective means of enabling random PRI staggering. Indeed, the larger SNR movers are easily observable and detectable, with additional gain sure to reveal the modest movers as well.

V. Conclusions

The RISR form of RMMSE adaptive processing has been formulated for adaptive Doppler estimation and then applied to uniform and staggered PRI pulse arrangements, both without and with clutter cancellation. Staggering facilitates the extension of unambiguous Doppler as a trade-off for higher sidelobes, which are then compensated by adaptive estimation. Open-air data demonstrates the prospect of enhanced discernibility of movers and subsequent detection performance benefits.

References

[1] M.A. Richards, J.A. Scheer, W.A. Holm, *Principles of Modern Radar: Basic Principles*, SciTech Publishing, 2010.

[2] R. Roy, O. Lowenschuss, "Design of MTI detection filters with nonuniform interpulse periods," *IEEE Trans. Circuit Theory*, vol. 17, no. 4, pp. 604-612, Nov. 1970.

[3] R.J. McAulay, "The effect of staggered PRF's on MTI signal detection," *IEEE Trans. Aerospace & Electronic Systems*, vol. AES-9, no. 4, pp. 615-618, July 1973.

[4] R. Benjamin, "Form of doppler processing for radars of random p.r.i. and r.f. ," *Electronics Letters*, vol. 15, no. 24, pp. 782, Feb. 1979.

[5] S.B. Rasool, M.R. Bell, "Efficient pulse-Doppler processing and ambiguity functions of nonuniform coherent pulse trains," *IEEE Radar Conf.*, Washington, DC, May 2010.

[6] Z. Liu, X. Wei, X. Li, "Aliasing-free moving target detection in random pulse repetition interval radar based on compressed sensing," *IEEE Sensors Journal*, vol. 13, no. 7, pp. 2523-2534, July 2013.

[7] J. Zhu, T. Zhao, T. Huang, D. Zhang, "Analysis of random pulse repetition interval radar," *IEEE Radar Conf.*, Philadelphia, PA, May 2016.

[8] T. Fan, Y. Kong, M. Wang, X. Yu, G. Cui, L. Zhang, "Doppler filter bank design for non-uniform PRI radar in signal-dependent clutter," *IEEE Radar Conf.*, Atlanta, GA, May 2021.

[9] W. van Rossum, L. Anitori, "Simultaneous resolution of range-Doppler ambiguities using agile pulse intervals with sparse signal processing," *IEEE Radar Conf.*, Washington, DC, Apr. 2020.

[10] S.D. Blunt, K. Gerlach, "Adaptive pulse compression via MMSE estimation," *IEEE Trans. Aerospace & Electronic Systems*, vol. 42, no. 2, pp. 572-584, April 2006.

[11] D. Henke, P. McCormick, S.D. Blunt, T. Higgins, "Practical aspects of optimal mismatch filtering and adaptive pulse compression for FM waveforms," *IEEE Intl. Radar Conf.*, Washington, DC, May 2015.

[12] L. Harnett, D. Hemmingsen, P. McCormick, S.D. Blunt, C. Allen, A. Martone, K. Sherbondy, D. Wikner, "Optimal and adaptive mismatch filtering for stretch processing," *IEEE Radar Conf.*, Oklahoma City, OK, Apr. 2018.

[13] P.M. McCormick, S.D. Blunt, "Shared-spectrum multistatic radar: experimental demonstration using FM waveforms," *IEEE Radar Conf.*, Oklahoma City, OK, Apr. 2018.

[14] C.C. Jones, L.A. Harnett, C.A. Mohr, S.D. Blunt, C.T. Allen, "Structure-based adaptive radar processing for joint clutter cancellation and moving target estimation," *IEEE Intl. Radar Conf.*, Washington, DC, Apr. 2020.

[15] S.D. Blunt, T. Chan, K. Gerlach, "Robust DOA estimation: the reiterative superresolution (RISR) algorithm," *IEEE Trans. Aerospace and Electronic Systems*, vol. 47, no. 1, pp. 332-346, Jan. 2011.

[16] E. Hornberger, S.D. Blunt, T. Higgins, "Partially constrained adaptive beamforming for super-resolution at low SNR," *IEEE Intl. Workshop Computational Advances in Multi-Sensor Adaptive Processing*, Cancun, Mexico, Dec. 2015.

[17] C.C. Jones, Z.E. Gannon, D. DePardo, J.W. Owen, B.H. Kirk, S.D. Blunt, C.T. Allen, "Development & experimental assessment of robust direction finding and array self-calibration," *IEEE Radar Conf.*, New York, NY, Mar. 2022.

[18] C.C. Jones, S.D. Blunt, B.H. Kirk, "An adaptive spectrogram estimator for enhanced signal characterization," *IEEE Radar Conf.*, New York, NY, Mar. 2022